ADVANCED BIOSYSTEMS
www.adv-biosys.com

Universal Statistical Laws for the Velocities of Collective Migrating Cells

Shao-Zhen Lin, Peng-Cheng Chen, Liu-Yuan Guan, Yue Shao, Yu-Kun Hao, Qunyang Li, Bo Li, David A. Weitz, and Xi-Qiao Feng**

Migratory dynamics of collective cells is central to the morphogenesis of biological tissues. The statistical distribution of cell velocities in 2D confluent monolayers is measured through large-scale and long-term experiments of various cell types lying on different substrates. A linear relation is discovered between the variability and the mean of cell speeds during the jamming process of confluent cell monolayers, suggesting time-invariant distribution profile of cell velocities. It is further found that the probability density function of cell velocities obeys the non-canonical *q*-Gaussian statistics, regardless of cell types and substrate stiffness. It is the Tsallis entropy, instead of the classical Boltzmann–Gibbs entropy, that dictates the universal statistical laws of collective cell migration. The universal statistical law stems from cell–cell interactions, as demonstrated by the wound healing experiments. This previously unappreciated finding provides a linkage between cell-level heterogeneity and tissue-level ensembles in embryonic development and tumor growth.

1. Introduction

Collective motions widely occur in complex material systems (e.g., sand dunes[1] and active nematics[2,3]) and biological systems (e.g., fishes,[4] insects,[4] bacteria,[5,6] and cells[7–14]). Rich geometric patterns can be observed in these collective moving systems, as a result of minimization of energy dissipation or other physical mechanisms.[15–17]

Collective and coordinated cell migration plays a key role in many physiological and pathological processes, for examples, embryonic morphogenesis, wound healing, and cancer invasion and metastasis.[18–23] Collective cell migration often manifests a heterogeneous but coordinated landscape.[5,7,9,24–26] In addition, the dynamic behaviors of cells vary vastly for different cell types and under different environments.[7,9,24–29]

Statistical mechanics provides a powerful tool to understand the motion of cells. For example, it has been successfully applied to understand the motion of isolated cells that undergo uncoordinated migration.[30,31] Cell velocity is one of the most important parameters that govern the dynamic behaviors of collective motions. The statistical features of cell velocities greatly influence the formation and transition of various migration modes and geometric patterns in self-organizing multicellular assemblies. However, the statistical law for the velocities of collective migratory cells remains unclear. Here we perform a series of large-scale and long-term experiments on confluent cell monolayers of various cell types adhering on different substrates and investigate the statistical distribution of cell velocities for collective cell migration. The variability and mean of cell speeds are found to follow a linear relation, suggesting a time-invariant distribution of cell velocities during the experimental duration. Somewhat surprisingly, our measurements show that the probability density function (PDF) of cell velocities does not follow either the traditional Gaussian distribution or the *k*-gamma distribution which the cell shapes in epithelial tissues obey.[32] Instead, our experiments suggest that the PDF of cell velocities obeys the *q*-Gaussian distribution, which is elucidated by using the concept of Tsallis entropy. The distribution parameter q, called the entropic index, keeps unchanged during the experimental duration though cell motions gradually slow down. Intriguingly, the *q*-Gaussian distribution of cell velocities has been verified for all cell monolayers we have measured, with a similar entropic index $q \approx 1.2$. We further reveal that the *q*-Gaussian distribution of cell velocities is insensitive to the substrate stiffness. In addition, our wound healing assay indicates that the *q*-Gaussian distribution of cell velocities stems from cell–cell interactions. Our findings suggest that the dynamic behaviors of living cell systems can be better explained by the non-extensive Tsallis

Dr. S.-Z. Lin, Dr. P.-C. Chen, Dr. L.-Y. Guan, Prof. Y. Shao, Dr. Y.-K. Hao, Prof. B. Li, Prof. X.-Q. Feng
Institute of Biomechanics and Medical Engineering
Department of Engineering Mechanics
Tsinghua University
Beijing 100084, China
E-mail: libome@tsinghua.edu.cn; fengxq@tsinghua.edu.cn
Prof. Q. Li
AML
Department of Engineering Mechanics
Tsinghua University
Beijing 100084, China
Prof. D. A. Weitz
School of Engineering and Applied Sciences
Harvard University
Cambridge, MA 02138, USA
The ORCID identification number(s) for the author(s) of this article can be found under https://doi.org/10.1002/adbi.202000065.

DOI: 10.1002/adbi.202000065

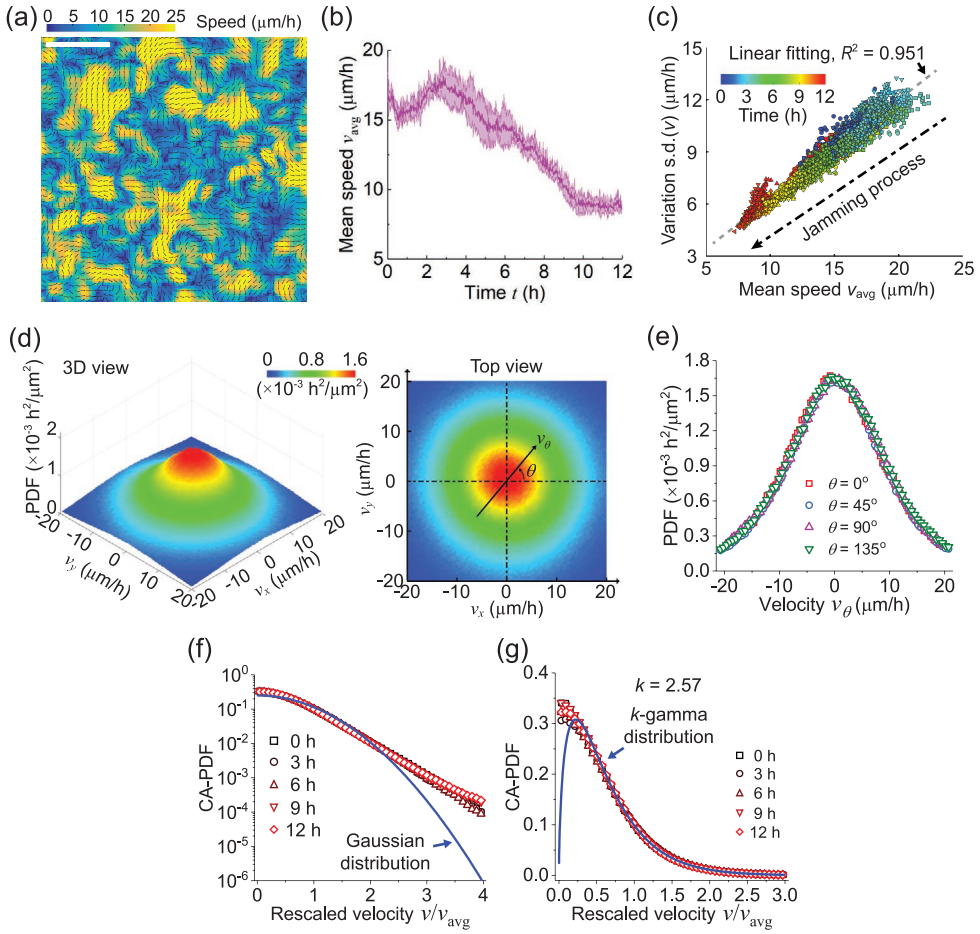

Figure 1. The PDF of cell velocities in the MDCK cell monolayer. a) Representative velocity field. Black arrows show velocity directions, and the color code indicates the magnitude. Scale bar, 300 μm. b) Temporal evolution of the mean speed of cells over the FOV. Shown here is the mean ± SD. c) Scatter diagram of the variation s.d.(v) versus the mean v_{avg} of cell speeds over time. Each data point represents [v_{avg}, s.d.(v)] in the FOV at time t. Symbols indicate independent FOVs (n = 6) and the color code indicates time. d) PDF of cell velocities. e) Cross-sectional plots along different orientations of the PDF profile of cell velocities shown in (d). Here, v_θ is the velocity component along the θ direction. f) Comparison between the PDF of cell velocities and the Gaussian distribution. g) Fitting the PDF of cell velocities to the k-gamma distribution via MLE, with the parameter k = 2.57.

statistical mechanics theory than the traditional Boltzmann–Gibbs theory. The entropic index q provides a possible measure to quantify the intrinsic cell–cell interactions in moving cell collectives.

2. Results and Discussion

To generate multicellular monolayer systems, Madin Darby canine kidney (MDCK) cells are seeded on 35 mm Petri dishes and cultured for 12–24 h to reach confluence with cell density around 140 000 cm^{-2}. Time-lapse phase contrast images, containing around 2500 cells in each field of view (FOV), are then taken for the monolayer during the subsequent 12 h (see Section 4 for detailed experimental methods). To assess the statistics of collective cell motion, we measure the velocities of all cells throughout the experimental duration using particle image velocimetry (PIV) analysis (see Section 4). The velocity field reveals the formation of swirl-like patterns with a characteristic size of several cells (**Figure 1**a, and see Movie S1, Supporting Information). The cell velocities manifest a distinct spatial heterogeneity: some cells are grouped together to form local cell packs that move and swirl collectively.[7,9] As the MDCK monolayer matures and becomes denser over time, it undergoes a jamming process,[10] where cells become progressively caged by their neighbors and their motion speeds decrease non-monotonically with time (Figure 1b).

Importantly, our data show that in the MDCK monolayer, the mean value v_{avg} and the standard deviation s.d.(v) of cell speeds follow a linear relation, s.d.(v) = 0.571v_{avg} + 0.580, with the correlation coefficient R^2 = 0.941 (Figure 1c), which suggests a time-invariant statistical distribution of cell velocities. To further validate this finding, we examine the PDF of cell velocities, $p_{vel}(\mathbf{v})$ (see Section 4 for detailed calculation methods), which is unimodal with the peak at $\mathbf{v} = \mathbf{0}$ and decreasing with speed $v = |\mathbf{v}| = \sqrt{v_x^2 + v_y^2}$ (Figure 1d). Notably, the PDF exhibits an isotropic profile (Figure 1d), as reflected by the identical cross-sectional landscape of $p_{vel}(\mathbf{v})$ in all directions (Figure 1e). Due to this isotropic feature, the 3D PDF landscape of $p_{vel}(\mathbf{v})$ can be fully represented by a 2D, circumferentially

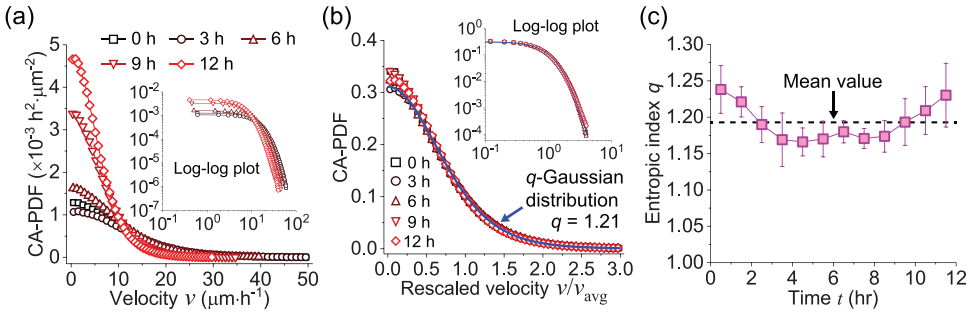

Figure 2. The PDF of cell velocities in the MDCK cell monolayer obeys the *q*-Gaussian distribution. a) Evolution of CA-PDFs for cell velocities with time. Inset: log–log plot of the CA-PDFs. b) CA-PDFs of the rescaled cell velocities at different time collapse to a family of PDFs, which can be well fitted by the *q*-Gaussian distribution. Inset: log–log plot of the CA-PDFs. c) Temporal fluctuation of the measured entropic index *q*. Error bars represent standard deviation (SD).

averaged PDF (CA-PDF) profile, $\overline{p}_{\rm vel}(v)=\frac{1}{2\pi}\int_{|\mathbf{v}|=v} p_{\rm vel}(\mathbf{v})\,{\rm d}\theta$, defined as the average of $p_{\rm vel}(\mathbf{v})$ over all directions $\theta=\arg(\mathbf{v})$ of cell velocities $\mathbf{v}$ at a specified speed v. As expected, the CA-PDFs of cell velocities at different time points exhibit similar landscapes (**Figure 2**a). To probe whether this distribution law $p_{\rm vel}(\mathbf{v})$ is time-invariant or not, we rescale the cell velocities by the average cell speed over the whole FOV and a time window of 1 h (from $t-0.5$ h to $t+0.5$ h) as $v_{\rm avg}=\frac{1}{A_{\rm FOV}}\int_{-0.5}^{0.5}{\rm d}s\int_{\rm FOV}v(\mathbf{x},t+s)\,{\rm d}\mathbf{x}$, where $A_{\rm FOV}$ is the area of FOV. We calculate the averaged cell speed over time based on the following considerations. On one hand, the average cell speed over the whole FOV at each time keeps nearly unchanged within this relatively short time window (Figure 1b). On the other hand, we have enough data sets (60 image slides) to construct the PDF of cell velocities. Subsequently, we calculate the CA-PDFs $\overline{p}_{\rm vel}(\tilde{v})$ of the rescaled velocity $\tilde{v}=|\tilde{\mathbf{v}}|$ with $\tilde{\mathbf{v}}=\mathbf{v}/v_{\rm avg}$ being the rescaled velocity. Our experimental data clearly show that all rescaled CA-PDFs of cell velocities collapse to a single, conserved distribution profile (Figure 2b), revealing a time-invariant statistical feature underlying the collective cell migration in the MDCK cell monolayer system.

We compare our experimental results with the Gaussian distribution adopted in a previous study.[33] Our results clearly show that the velocity distribution deviates from the Gaussian distribution, especially in the scope of larger velocities (Figure 1f), suggesting a non-Gaussian distribution of cell velocities. In addition, it has been found that the aspect ratios of cells in epithelial tissues obey the *k*-gamma distribution.[32] We wonder whether the cell velocities satisfy the *k*-gamma distribution or not. Figure 1g shows that the *k*-gamma distribution does not fit the cell velocity distribution profile, suggesting a dynamic statistics distinct from that for cell shapes. Further, our experimental data for the cell velocity distributions in the log–log plot do not follow a linear law and thus deviate distinctly from the power law distribution (Figure 2a,b).

Of note, the power-law tail feature of cell velocity distribution (Figure 2a,b) is reminiscent of the *q*-Gaussian distribution observed in some non-living systems.[34–36] Then a question raises naturally: Does the velocities of the MDCK cells in a monolayer system follow the same *q*-Gaussian statistical law? To answer this question, we fit the rescaled cell velocities to the *q*-Gaussian distribution through the maximum likelihood estimation (MLE; see Section 4). As shown in Figure 2b, the MDCK cell velocity distribution indeed closely matches the *q*-Gaussian distribution:

$$f_{q-G,2D}(\tilde{\mathbf{v}};q)=A_q\left(1+B_q|\tilde{\mathbf{v}}|^2\right)^{-\lambda_q} \tag{1}$$

where $\lambda_q=1/(q-1)$, $A_q=(1/\pi)(\lambda_q-1)B_q$, and $B_q=(\pi/4)\left[\Gamma\left(\lambda_q-\frac{3}{2}\right)/\Gamma(\lambda_q-1)\right]^2$, with $\Gamma(\cdot)$ being the Legendre gamma function (see Supporting Information). The *q*-Gaussian distribution in non-extensive statistical physics is a generalization of the traditional Gaussian distribution. The former contains one more parameter, *q*, called the entropic index, which quantifies the non-extensivity or correlations of the system. *q* determines the profile of the *q*-Gaussian distribution: in the limiting case of $q\to 1$, the *q*-Gaussian distribution asymptotically approaches the traditional Gaussian distribution (see Supporting Information). By analyzing the data set via MLE, it renders an entropic index, $q=1.183\pm0.035$ (mean±SD), with small fluctuations throughout the jamming process in the MDCK monolayer (Figure 2c). Thus, the above results provide a time-independent quantitative statistical property of morphogenetic cell motion.

Next, we examine the statistics of cell velocity gradients, which correspond to the strain rate in confluent cell monolayers. For example, the vorticity $\omega=\partial v_y/\partial x-\partial v_x/\partial y$ reflects the strength of cellular swirling. Our data show that the vorticity fields at different time points exhibit similar landscapes (Figure S1a, Supporting Information). Rescaling the vorticity as $\tilde{\omega}=\omega/\omega_{\rm rms}$ with $\omega_{\rm rms}=\sqrt{\langle\omega^2\rangle}$ being the root-mean-square vorticity, we find that the rescaled vorticity field at different time points collapse to a common PDF profile (Figure S1b, Supporting Information). To investigate whether the *q*-Gaussian statistics can be extended to quantify the distribution of cell vorticities, we fit the rescaled cell vorticities to the 1D *q*-Gaussian distribution through MLE (see Section 4). It is found that the PDF of the rescaled vorticity truly obeys the 1D *q*-Gaussian distribution,

$$f_{q-G,1D}(\tilde{\omega};q)=\frac{C_q}{\left(1+D_q\tilde{\omega}^2\right)^{\lambda_q}} \tag{2}$$

where $C_q = \Gamma(\lambda_q)\Big/\left[\sqrt{\pi(2\lambda_q-3)}\Gamma\left(\lambda_q-\frac{1}{2}\right)\right]$ and $D_q = 1/(2\lambda_q-3)$ (Figure S1b, Supporting Information). This suggests that the statistics of mechanical stresses in the moving cell collectives may also follow the q-Gaussian distribution, thus identifying a unique, previously unrecognized statistical nature for the physical forces in collective cell migration.[37] Importantly, the q index determined from the vorticity distribution matches that determined from the velocity distribution (Figure S1c, Supporting Information), thereby further confirming the conserved nature of the q-Gaussian statistics underlying the self-organizing cell flows.

Now it is of special interest to examine whether the q-Gaussian statistics in Equation (1) works only for MDCK cells under specific conditions or is a universal law that governs the collective migration of other cells. Therefore, more systematic experiments are performed for some other representative epithelial and mesenchymal cell types, including human umbilical vein endothelial cells (HUVECs), C2C12 mouse myoblasts (C2C12), and NIH-3T3 mouse embryo fibroblast (NIH-3T3). These cells show drastically different biological and mechanical properties. For example, C2C12 and NIH-3T3 cells exhibit much weaker motility than MDCK and HUVEC (**Figure 3**a). However, our experiments show that the swirling migration pattern (Movies S2–S4, Supporting Information) and the isotropic PDF of velocities are conserved across all these cell types.

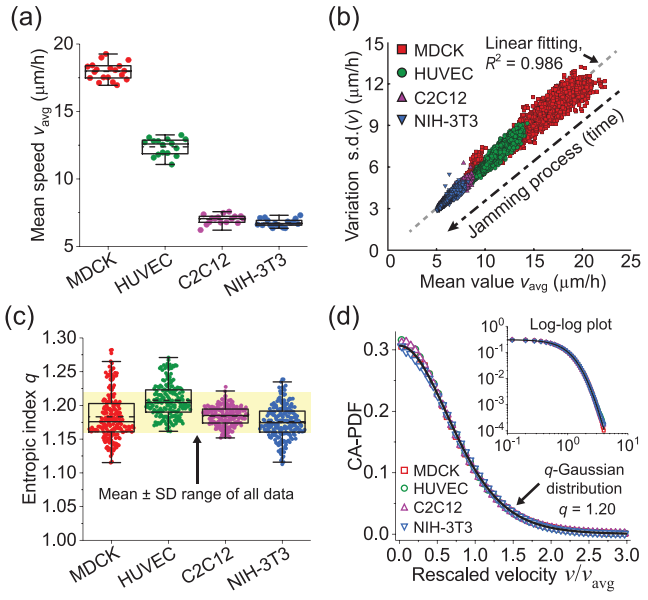

Figure 3. Universal q-Gaussian statistics for the velocities of diverse cell types collectively migrating in a monolayer. a) The mean speed v_{avg} measured from the monolayers of different cell types with a similar cell density (≈140 000 cm^{-2}) over a time window of 1 h. b) Scatter diagram of the variation s.d.(v) versus the mean v_{avg} of cell speeds in the monolayers of different cell types. All data points [v_{avg}, s.d.(v)] were measured from the FOV. Here, the dot-dashed arrow indicates the time evolution direction as well as a jamming process. c) Values of the entropic index q calculated across different cell types. In (**a**) and (**c**), box plots: solid line, median; dashed line, mean; box, interquartile range; whiskers, 1.5× interquartile range. The yellow area represents mean ± SD range of all data. d) CA-PDFs of rescaled velocities of different cell types collapse to the same conserved profile of the q-Gaussian statistical distribution.

More importantly, during the jamming process in all monolayer systems, the variability s.d.(v) and the mean v_{avg} of cell speeds follow the same linear relation we have observed in the MDCK sample (Figure 3b). Thus this finding suggests a universal statistical law for collective cell migration, regardless of cell types. Despite the dispersion of motility and other properties of different cell types (Figure 3a), their velocities closely match the time-invariant q-Gaussian statistical distribution function (Figure S2, Supporting Information). The only small difference in their velocity statistics lies only in their values of entropic index: q = 1.208 ± 0.025 for HUVEC, q = 1.184 ± 0.014 for C2C12, and q = 1.176 ± 0.024 for NIH-3T3, compared with q = 1.183 ± 0.035 for MDCK (Figure 3c). Obviously, the statistical distribution profiles of rescaled velocities in all cell systems well collapse into the same q-Gaussian landscape (Figure 3d). Therefore, our experiments reveal a universal, invariant statistics of collective cell velocities in monolayer systems, and the dynamics of all collective migratory cells obeys the q-Gaussian statistics, with the entropic index keeping consistent over time and conserved over various cell types.

As is well known, extracellular matrix plays a key regulating role in the dynamic behaviors of cells, both in vitro[38–40] and in vivo.[41,42] For example, substrate stiffness may significantly affect the velocity and persistence of cell migration.[24,39] Therefore, it is of interest to investigate whether the mechanical properties of the substrate underlying the collective cells would or not interfere with the statistical law we have discovered above. To this end, we measure MDCK cells on different substrates (see Section 4), including polyacrylamide (PA) gels, polydimethylsiloxane (PDMS), plastics, and glasses, whose Young's moduli span from 10 kPa to 70 GPa. For comparison of collective cell migration on these substrate, one may refer to the Movies S5–S8, Supporting Information. Indeed, a remarkable difference can be observed in the motility of the MDCK cells on different substrates. As shown in **Figure 4**a, the average cell migration speed increases with substrate stiffness, in consistency with previous studies.[39,43] Nonetheless, the statistical distribution of rescaled cell velocities keeps unchanged with the increase in substrate stiffness and always matches the q-Gaussian function in Equation (1) (Figure 4c and Figure S3, Supporting Information), except that the measured entropic index q shows a small change of no more than 10%, in great contrast to the large variation in the substrate stiffness across six orders of magnitude (Figure 4b). This suggest that the q-Gaussian distribution statistics of cell velocities in cell monolayer systems is insensitive to substrate rigidity.

Recent studies have demonstrated the role of boundary constraints in modulating collective cell migration, such as inducing collectively directed motion[8,44–46] or persistent angular rotations in a confined space.[47–50] Would the existence of free boundaries, which represent the case of wounding, change the q-Gaussian statistics of collective cell flows? To address this issue, we explore the statistics of collective cell flows in the presence of a straight free boundary in the MDCK monolayer. In this case, cells tend to move toward the free boundary, guided by leader cells that extend active protrusions into the free space (**Figure 5**a and Movie S9, Supporting Information). PIV analysis illustrates that the mean speed of cells decreases at locations away from the free boundary (Figure 5b). The biased migration

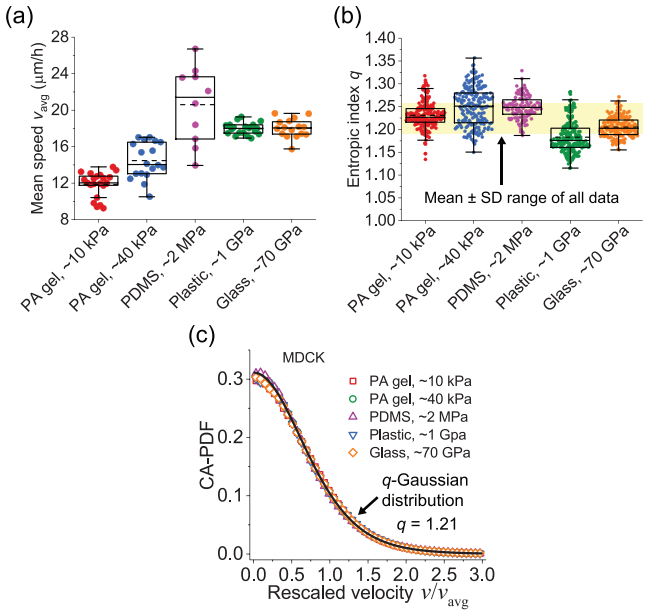

Figure 4. Substrate stiffness does not interfere with the q-Gaussian statistics of collective cell dynamics. a) The mean speeds of collective MDCK cells on substrates of different stiffnesses. b) The entropic index q for collective MDCK cells on substrates of different stiffnesses. The yellow area represents mean ± SD range of all data. c) The CA-PDF profiles of the rescaled cell velocities in MDCK monolayers on different substrates all collapse to the q-Gaussian distribution with $q \approx 1.21$.

of cells toward the free space results in an anisotropic PDF profile of cell velocities (Figure 5c). Based on the distance d_b to the free boundary, we divide the cell monolayer into several regions and examine the PDFs of cell velocities in each. Our results show that in the vicinity of the free boundary (e.g., $0 < d_b < 250$ μm), the distribution of cell velocities exhibits notable anisotropy and is skewed markedly from the q-Gaussian distribution (Figure 5d). Departing from the free boundary, however, the distribution of cell velocities gradually recovers to the q-Gaussian distribution. Correspondingly, the apparent entropic index increases from $q = 1.09$ in the vicinity of free boundary to $q = 1.22$ in the inner region of the cell monolayer (Figure 5e). This is probably due to the increase in the mutual constraints of cellular motions when approaching the denser inner regions. The effective distance within which the free boundary poses a notable influence on the statistics of collective cell flows is estimated to be around $d_{eff} \approx 500$ μm for MDCK cell monolayers, which is about two times of the swirl size. These results demonstrate that boundary constraints have a distinct influence on the statistics of collective cell flows. The q-Gaussian statistics thus reflects a unique homeostatic state of cell ensembles, which can be skewed upon breakage of the continuum of cell collectives. This suggests that the q-Gaussian statistical distribution of cell velocities in confluent monolayers, as well as the entropic index, are related to cell–cell interactions.

We next explore the physical mechanisms underlying the universality of the q-Gaussian statistical law of collective cells. The negligible effects of substrate stiffness suggest that the highly conserved q-Gaussian statistics of cell velocities stems

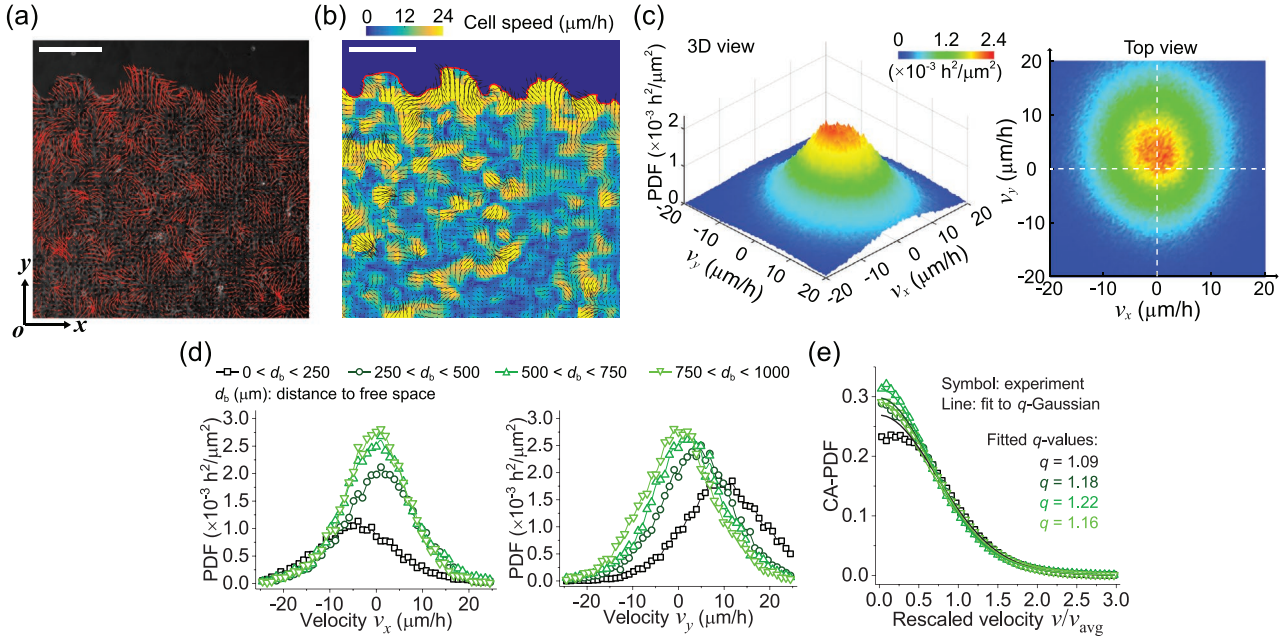

Figure 5. The q-Gaussian statistics of cell dynamics is skewed by free boundaries. a) Representative image of a scratched MDCK cell monolayer. Arrows indicate velocity vectors. b) Heat map of the velocity field shown in (a). Arrows represent velocity vectors, and the color code indicates velocity magnitude; the red line donates the free boundary. c) The PDF of cell velocities in the whole FOV. d) PDFs of cell velocities in different regions of different distance d_b to the free boundary. e) CA-PDFs of rescaled cell velocities in different regions defined in (d). Here, the rescaled cell velocity is calculated based on the average speed corresponding to each region. Each data point represents experimental measurements. The solid lines represent q-Gaussian fitting with entropic indices noted in the plot. Scale bars, 300 μm.

mainly from cell–cell interactions, which involve complicated coupling mechanical and chemical cues. This is further evidenced by our wound healing experiments demonstrated above (Figure 5), which show that exogenously induced free boundaries can skew the q-Gaussian statistics of otherwise homeostatic monolayers.

In statistical physics, the Boltzmann–Gibbs entropy

$$S_{\mathrm{BG}} = -k_{\mathrm{B}} \int p(x) \ln [p(x)] \, \mathrm{d}x \tag{3}$$

has been widely applied to stochastic processes in thermodynamic equilibrium systems, where k_{B} is the Boltzmann constant, and $p(x)$ is the probability distribution function of variable x. However, analysis of our experimental data shows that the classical theory of Boltzmann–Gibbs entropy cannot interpret the universal statistical laws of collective cell migration. This is because the Boltzmann–Gibbs entropy ignores the interactions and correlations between individuals, and thus is not exact for confluent cell monolayers, where cell motions are strongly correlated due to the coupled mechanical and chemical interactions between neighboring cells. Moreover, living cell systems are often non-equilibrium due to active motility of cells driven by sustaining energy input (e.g., ATP hydrolysis).

In this work, therefore, we utilize the theory of Tsallis entropy, which is defined as

$$S_q = \frac{k_{\mathrm{B}}}{q-1} \left\{ 1 - \int [p(x)]^q \, \mathrm{d}x \right\} \tag{4}$$

where the entropic index q quantifies the non-extensivity of the system. Tsallis entropy S_q in Equation (4) is a generalization of Boltzmann–Gibbs entropy S_{BG} in Equation (3). In the limiting case of $q \to 1$, it reduces to S_{BG}. The q-Gaussian distribution in Equation (1) can be derived as a product of optimizing Tsallis entropy under normalization and mean energy constraints.[51] In comparison with the Boltzmann–Gibbs entropy, the Tsallis entropy takes the effects of intercellular interactions and correlations into account. Tsallis entropy have been applied extensively to capture the statistical features of complex systems that are out of equilibrium or confer strong correlations,[52] for example, cold atoms in dissipative optical lattices,[34] driven dissipative dusty plasma,[35] and spin-glasses.[36] By applying the theory of Tsallis entropy to the multicellular monolayer systems under study, we can easily find that the cell velocities follow the q-Gaussian distribution. Our experiments of diverse cell types demonstrate the applicability of Tsallis entropy to multicellular systems. In addition, it is emphasized that the entropic index q provides a new measure to quantify the intrinsic interactions of moving cell collectives.

3. Conclusions

In summary, we have performed a series of large-scale experiments of various cell types to investigate the statistics of cell velocities in 2D confluent monolayers. Our experiments have revealed that the cell velocities and vorticities conform to the q-Gaussian statistical distribution, rather than the standard Gaussian[30] and exponential[31] distributions previously demonstrated for isolated migrating cells. The q-Gaussian statistical law is shown to be universal for various morphogenetic cell motions: it is independent of cell types, time, and substrate stiffness. Further, our wound healing experiments revealed that the q-Gaussian statistics of cell velocities arises from complex cell–cell interactions. Thus our experimental data suggest the applicability of Tsallis entropy theory in multicellular systems. Our analysis establishes two key physical parameters to evaluate the non-extensivity of the entropy of multicellular systems: the entropic index q and the linear coefficient k between the variability and the mean of cell speeds. These findings deepen our physical understanding of collective morphogenetic cells in 2D monolayers.

Finally, it is worth mentioning some perspective extensions of this work. First, the present study focuses on the distribution of cell velocities in cell monolayer systems. It is of interest to examine the evolution of cell velocity distribution profile during the formation of confluent cell monolayers from isolated cells. Besides, a recent study showed that in monolayers of MCF10A cell line, cell persistence exhibited poor relevance to both cell speed and cell shape.[53] This suggests that the cell persistence may not follow the q-Gaussian distribution as cell velocities, or the k-gamma distribution recently found for cell shapes in epithelial tissues.[32] These inferences need to be verified by experiments. In addition, the universality of q-Gaussian statistics to cell migration in 3D environments deserves experimental and theoretical efforts.

4. Experimental Section

Cell Culture and Live-Cell Imaging: MDCK strain II cells were cultured in a culture medium composed of high glucose DMEM (Corning) supplemented with 10% fetal bovine serum (FBS, Gibco) and 1% antibiotics solution (100 μg mL^{-1} penicillin +100 μg mL^{-1} streptomycin; Gibco). HUVECs were cultured in DMEM/F12 (Gibco) supplemented with 10% FBS (Gibco) and 1% antibiotics solution (100 μg mL^{-1} penicillin + 100 μg mL^{-1} streptomycin; Gibco). C2C12 myoblasts cells and NIH-3T3 fibroblasts were cultured in DMEM (High glucose + GlutaMAX; Gibco) supplemented with 10% FBS (Gibco) and 1% antibiotics solution (100 μg mL^{-1} penicillin + 100 μg mL^{-1} streptomycin; Gibco). All cells were incubated at 37 °C with 5% CO_2.

To explore the role of substrate stiffness in the distribution statistics of cell velocities in 2D cell monolayer systems, we cultured cells on substrates with different stiffnesses. Substrates used in our experiments included polyacrylamide (PA) gels, polydimethylsiloxane (PDMS), plastics, and glasses. PA gel substrates, whose stiffness can be tailored by adjusting the concentrations of monomers and cross-linkers, were prepared according to the standard protocols reported previously.[54,55] Specifically, we manufactured PA gels of stiffnesses ≈10 kPa and 40 kPa, using ratios of acrylamide (Sigma, 40% w/v) to bis-acrylamide (Sigma, 2% w/v) as suggested in previous protocols.[54,55] The PA gel substrates were functionalized with collagen I (500 μg mL^{-1}) before seeding cells. To make PDMS substrates (Sylgard 184; Dow Corning) with stiffness of ≈2 MPa,[56] the base and curing agent were first mixed with a ratio of 10:1 (w/w), followed by degassing in a vacuum chamber, after which a thin layer of PDMS was spin-coated over a 35 mm Petri dish, degassed again and cured at 80 °C for 2 h. The PDMS-coated Petri dish was exposed to UV for 30 min and functionalized with fibronectin (Corning, 50 μg mL^{-1}) before seeding cells. Cells were also cultured directly on 35 mm plastic Petri dishes (Corning) which represent rigid substrate with stiffness ≈1 GPa. In addition, cells were cultured on a 35 mm glass-bottom confocal Petri dish (Corning), where the glass bottom has stiffness ≈70 GPa.

To study collective cell migration, a confluent monolayer was allowed to develop on various substrates as mentioned above for enough time (typically 12–24 h) to reach final cell density ≈140 000 cm^{-2}. Subsequently, phase contrast images were acquired using an Olympus IX83 inverted fluorescence microscope with a 10× objective. The size of the FOV is 1.33 mm × 1.33 mm, much larger than the spatial correlation length (200–300 μm) of collective cell migration, and thus sufficient for analyzing the statistics of collective cell motions. Successive images of the same FOV were taken at a time interval of 1 min, with a total duration longer than 12 h.

Particle-Image-Velocimetry Analysis: Particle-image-velocimetry (PIV) analysis was performed to obtain the velocity field of collective cell flows.[10,24] Raw phase contrast images were first pre-processed by contrast enhancement followed by high-pass Gaussian filtering to conserve the high frequency component and remove the background noise, with the kernal size of ≈1 cell (≈20 pixels in length). The velocity field was then computed from these pre-processed images using PIV. In the cross-correlation calculation of PIV, the interrogation window size was taken as 48 × 48 pixels, which roughly corresponded to a region of 2 × 2 cell length. Outliers of the obtained velocity vectors were abolished and replaced by fitting values based on the neighboring velocity vectors. The velocity gradient field was calculated based on the extracted velocity field via least-squares method. Custom-made PIV software was written in MATLAB.[57]

For the cell monolayer with a free boundary, the velocity field in the whole FOV was calculated and then the velocity vectors outside the cell monolayer were excluded. The free boundary was extracted automatically via a user-developed MATLAB script: i) the raw phase contrast images were first converted to binary images based on a manually selected threshold (using the MATLAB built-in function "imbinarize"); ii) the binary images were treated by morphologically opening (using the MATLAB built-in function "imopen") and morphologically closing (using the MATLAB built-in function "imclose") operations to remove impurities in the free space region and construct coherent domains in the cell monolayer region; iii) small coherent regions outside the coherent cell monolayer region were removed; iv) after filling the holes in the cell monolayer region (using the MATLAB built-in function "imfill"), the free boundary of cell monolayer was extracted (using the MATLAB built-in function "bwboundaries"). To improve the performance of such automatic algorithm, we plotted the extracted free boundaries on the raw images and adjusted the manually selected parameters accordingly.

Calculation of the PDFs of Cell Velocities and Vorticities: The data set for calculating the PDFs of cell velocities and vorticities were obtained via PIV analysis on the consecutive phase contrast image series. To calculate the PDF at a time point t, the data set of velocity field during a time window of 1 h was collected, that is, the time interval [t − 0.5 h , t + 0.5 h]. Since the average cellular motion speed did not vary apparently (see Figure 1b), it could be assumed that pseudo-ergodicity of collective cell flows during this time window. From the PIV analysis, there were 196 × 196 data set points of the velocity field for each image slide. Besides, 60 images were taken during live-cell imaging of a time window of 1 h (time interval = 1 min) . Accordingly, the number of collected data set points during the time window was $N_{\text{dataset}} = 196 \times 196 \times 60 = 2,304,960$, sufficiently large for the calculation of PDFs.

To calculate the PDF of cell velocities, we first constructed a regular grid in the 2D velocity space, with the grid points represented as $(v_x^{(1)}, v_x^{(2)}, \ldots, v_x^{(m+1)}) \times (v_y^{(1)}, v_y^{(2)}, \ldots, v_y^{(n+1)})$, where $v_x^{(1)}, v_x^{(2)}, \ldots, v_x^{(m+1)}$ and $v_y^{(1)}, v_y^{(2)}, \ldots, v_y^{(n+1)}$ are series of velocity components along the x and the y directions, respectively, and equally spaced with $v_x^{(i+1)} - v_x^{(i)} = \Delta v_x$ and $v_y^{(j+1)} - v_y^{(j)} = \Delta v_y$. In our calculations, typically the series of velocity components were set as $v_x^{(1)} = v_y^{(1)} = -30\ \mu\text{m h}^{-1}$ and $v_x^{(m+1)} = v_y^{(n+1)} = +30\ \mu\text{m h}^{-1}$, and the number of velocity intervals $m = n = 100$. We then counted the number of data set points $N_{i,j}$ in each velocity grid block $(v_x^{(i)}, v_x^{(i+1)}) \times (v_y^{(j)}, v_y^{(j+1)})$, leading to the occurrence frequency $O_{i,j} = N_{i,j}/N_{\text{dataset}}$. Accordingly, the PDF of cell velocities at the grid point $(v_x^{(i+\frac{1}{2})}, v_y^{(j+\frac{1}{2})}) = ((v_x^{(i)} + v_x^{(i+1)})/2, (v_y^{(j)} + v_y^{(j+1)})/2)$ was calculated as $p_{\text{vel}}(v_x^{(i+\frac{1}{2})}, v_y^{(j+\frac{1}{2})}) = O_{i,j}/(\Delta v_x \Delta v_y)$. Further, to obtain the CA-PDF, the obtained PDF values associated with the grid points $(v_x^{(i+\frac{1}{2})}, v_y^{(j+\frac{1}{2})})$ were averaged over the circumferential direction in the velocity space. Given the isotropy of the cell flow field, the CA-PDF in the 1D speed space can be calculated more conveniently. Specifically, a regular grid in the 1D speed space was constructed, with the grid points represented as, $(v^{(1)}, v^{(2)}, \ldots, v^{(n+1)})$, where $v^{(1)}, v^{(2)}, \ldots, v^{(n+1)}$ is speed series and equally spaced with $v^{(i+1)} - v^{(i)} = \Delta v$. In calculation, the speed series were typically set as $v^{(1)} = 0$ and $v^{(n+1)} = 40\ \mu\text{m h}^{-1}$, and the number of speed intervals was set as $n = 100$. Then the number of dataset points N_i was counted in each speed interval $(v^{(i)}, v^{(i+1)})$, leading to the occurrence frequency $O_i = N_i/N_{\text{dataset}}$. Accordingly, the CA-PDF of cell velocities at the grid point $v^{(i+\frac{1}{2})} = (v^{(i)} + v^{(i+1)})/2$ was calculated as $p_{\text{vel}}(v^{(i+\frac{1}{2})}) = O_i/(2\pi v^{(i+\frac{1}{2})}\Delta v)$. These two means for calculating the CA-PDF of cell velocities gave consistent results for confluent cell monolayers without free boundaries; for the latter, the first means should be used.

Similarly, to calculate the PDF of cell vorticities, a regular grid in the 1D vorticity space was constructed, with the grid points represented as, $(\omega^{(1)}, \omega^{(2)}, \ldots, \omega^{(n+1)})$, where $\omega^{(1)}, \omega^{(2)}, \ldots, \omega^{(n+1)}$ is vorticity series and equally spaced with $\omega^{(i+1)} - \omega^{(i)} = \Delta\omega$. Typically the vorticity series was set as $\omega^{(1)} = -1\text{h}^{-1}$ and $\omega^{(n+1)} = +1\text{h}^{-1}$, and the number of vorticity intervals $n = 100$. Then the number of dataset points N_i was counted in each vorticity interval $(\omega^{(i)}, \omega^{(i+1)})$, resulting in an occurrence frequency $O_i = N_i/N_{\text{dataset}}$, and accordingly the PDF of cell vorticities at the grid point $\omega^{(i+\frac{1}{2})} = (\omega^{(i)} + \omega^{(i+1)})/2$ was calculated as $p_{\text{vort}}(\omega^{(i+\frac{1}{2})}) = O_i/\Delta\omega$.

Fitting the Data Set of Cell Velocities to the 2D q-Gaussian Distribution: For each data set of cell velocities, $\{\mathbf{v}_i\}_{i\,=\,1,\,2,\,\cdots,\,n}$, first the data was rescaled as $\tilde{\mathbf{v}}_i = \mathbf{v}_i/v_{\text{avg}}$, where $v_{\text{avg}} = (1/n)\sum_{i=1}^{n} v_i$ is the average cellular motion speed with $v_i = |\mathbf{v}_i|$. Since the experimentally measured 2D PDF of cell velocities $p_{\text{vel}}(\mathbf{v})$ exhibits an isotropic feature, $p_{\text{vel}}(\mathbf{v}) = p_{\text{vel}}(|\mathbf{v}|)$, the data set of rescaled cell velocities $\{\tilde{\mathbf{v}}_i\}_{i=1,2,\ldots,n}$ were fitted to the 2D q-Gaussian distribution [Equation (1)]. For the data set of rescaled cell velocities, $\{\tilde{\mathbf{v}}_i\}_{i=1,2,\ldots,n}$, the likelihood function is

$$L(\tilde{v}_i; q) = \prod_{i=1}^{n} \frac{A_q}{(1 + B_q \tilde{v}_i^2)^{\lambda_q}} \tag{5}$$

The MLE estimate of q is then given by seeking the maximum of the likelihood function with respect to q. Taking the derivative of $L(\tilde{v}_i; q)$ with respect to q and setting it equal to zero yields

$$n\frac{1}{A_q}\frac{\partial A_q}{\partial q} + \sum_{i=1}^{n}\left[\lambda_q^2 \ln(1 + B_q\tilde{v}_i^2) - \lambda_q \frac{\tilde{v}_i^2}{1 + B_q\tilde{v}_i^2}\frac{\partial B_q}{\partial q}\right] = 0 \tag{6}$$

that is,

$$\begin{aligned} &\frac{1}{(\lambda_q - 1)} + 2\left[\psi\left(\lambda_q - \frac{3}{2}\right) - \psi(\lambda_q - 1)\right] \\ &- \frac{1}{n}\sum_{i=1}^{n}\ln\left(1 + B_q\tilde{v}_i^2\right) - 2\lambda_q\left[\psi\left(\lambda_q - \frac{3}{2}\right) - \psi(\lambda_q - 1)\right]\frac{1}{n}\sum_{i=1}^{n}\frac{B_q\tilde{v}_i^2}{1 + B_q\tilde{v}_i^2} = 0 \end{aligned} \tag{7}$$

where $\psi(x) = \Gamma'(x)/\Gamma(x)$ is the polygamma function. The above equation with respect to q can be readily numerically solved.

Fitting the Data Set of Cell Vorticities to the 1D q-Gaussian Distribution: For each data set of cell vorticities, $\{\omega_i\}_{i\,=1,2,\cdots,n}$, the data was first rescaled as $\tilde{\omega}_i = \omega_i/\omega_{\text{rms}}$ with $\omega_{\text{rms}} = \sqrt{(1/n)\sum_{i=1}^{n}\omega_i^2}$ being the root-mean-square vorticity. Similarly, via MLE, the data set of rescaled cell vorticities, $\{\tilde{\omega}_i\}_{i=1,2,\ldots,n}$ was fitted to the 1D q-Gaussian distribution Equation (2). For the data set of rescaled cell vorticities, $\{\tilde{\omega}_i\}_{i=1,2,\ldots,n}$, the likelihood function is

$$L(\tilde{\omega}_i; q) = \prod_{i=1}^{n} \frac{C_q}{(1 + D_q\tilde{\omega}_i^2)^{\lambda_q}} \tag{8}$$

Taking the derivative of $L(\tilde{\omega}_i;q)$ with respect to q and equating it to zero yields

$$n\frac{1}{C_q}\frac{\partial C_q}{\partial q}+\sum_{i=1}^{n}\left[\lambda_q^2\ln\left(1+D_q\tilde{\omega}_i^2\right)-\lambda_q\frac{\tilde{\omega}_i^2}{1+D_q\tilde{\omega}_i^2}\frac{\partial D_q}{\partial q}\right]=0 \tag{9}$$

that is,

$$-D_q+\psi\left(\lambda_q\right)-\psi\left(\lambda_q-\frac{1}{2}\right)-\frac{1}{n}\sum_{i=1}^{n}\ln\left(1+D_q\tilde{\omega}_i^2\right)+2\lambda_q\frac{1}{n}\sum_{i=1}^{n}\frac{D_q^2\tilde{\omega}_i^2}{1+D_q\tilde{\omega}_i^2}=0 \tag{10}$$

The above equation with respect to q can be numerically solved readily.

Statistical Analysis: For each kind of cell monolayers under study, phase contrast images were obtained from at least four independent samples. For each sample, at least 5 independent FOVs were taken and analyzed. In the PIV analysis, raw phase contrast images were pre-processed by contrast enhancement and high-pass Gaussian filtering using MATLAB. All data are presented as means ± standard deviation (SD), or box plots showing median, mean and interquartile range.

Supporting Information

Supporting Information is available from the Wiley Online Library or from the author.

Acknowledgements

This work was supported by the National Natural Science Foundation of China (Grant Nos. 11620101001, 11921002, and 11922207).

Conflict of Interest

The authors declare no conflict of interest.

Keywords

cell velocities, collective cell migration, q-Gaussian distribution, statistical mechanics

Received: March 2, 2020
Revised: June 9, 2020
Published online: August 17, 2020

[1] H. Elbelrhiti, P. Claudin, B. Andreotti, *Nature* **2005**, *437*, 720.
[2] Y. Sumino, K. H. Nagai, Y. Shitaka, D. Tanaka, K. Yoshikawa, H. Chaté, K. Oiwa, *Nature* **2012**, *483*, 448.
[3] L. Giomi, *Phys. Rev. X* **2015**, *5*, 031003.
[4] T. Vicsek, A. Zafeiris, *Phys. Rep.* **2012**, *517*, 71.
[5] H. H. Wensink, J. Dunkel, S. Heidenreich, K. Drescher, R. E. Goldstein, H. Löwen, J. M. Yeomans, *Proc. Natl. Acad. Sci. USA* **2012**, *109*, 14308.
[6] Z. You, D. J. Pearce, A. Sengupta, L. Giomi, *Phys. Rev. X* **2018**, *8*, 031065.
[7] T. E. Angelini, E. Hannezo, X. Trepat, M. Marquez, J. J. Fredberg, D. A. Weitz, *Proc. Natl. Acad. Sci. USA* **2011**, *108*, 4714.
[8] X. Serra-Picamal, V. Conte, R. Vincent, E. Anon, D. T. Tambe, E. Bazellieres, J. P. Butler, J. J. Fredberg, X. Trepat, *Nat. Phys.* **2012**, *8*, 628.
[9] S. Garcia, E. Hannezo, J. Elgeti, J. F. Joanny, P. Silberzan, N. S. Gov, *Proc. Natl. Acad. Sci. USA* **2015**, *112*, 15314.
[10] J. A. Park, J. H. Kim, D. Bi, J. A. Mitchel, N. T. Qazvini, K. Tantisira, C. Y. Park, M. McGill, S. H. Kim, B. Gweon, J. Notbohm, R. StewardJr, S. Burger, S. H. Randell, A. T. Kho, D. T. Tambe, C. Hardin, S. A. Shore, E. Israel, D. A. Weitz, D. J. Tschumperlin, E. P. Henske, S. T. Weiss, M. Lisa Manning, J. P. Butler, J. M. Drazen, J. J. Fredberg, *Nat. Mater.* **2015**, *14*, 1040.
[11] L. H. Deng, X. Trepat, J. P. Butler, E. Millet, K. G. Morgan, D. A. Weitz, J. J. Fredberg, *Nat. Mater.* **2006**, *5*, 636.
[12] D. Bi, X. Yang, M. C. Marchetti, M. L. Manning, *Phys. Rev. X* **2016**, *6*, 021011.
[13] C. Malinverno, S. Corallino, F. Giavazzi, M. Bergert, Q. Li, M. Leoni, A. Disanza, E. Frittoli, A. Oldani, E. Martini, *Nat. Mater.* **2017**, *16*, 587.
[14] L. Yan, D. Bi, *Phys. Rev. X* **2019**, *9*, 011029.
[15] A. J. Liu, S. R. Nagel, *Annu. Rev. Condens. Matter Phys.* **2010**, *1*, 347.
[16] M. C. Marchetti, J. Joanny, S. Ramaswamy, T. Liverpool, J. Prost, M. Rao, R. A. Simha, *Rev. Mod. Phys.* **2013**, *85*, 1143.
[17] C. Bechinger, R. Di Leonardo, H. Löwen, C. Reichhardt, G. Volpe, G. Volpe, *Rev. Mod. Phys.* **2016**, *88*, 045006.
[18] S. Z. Lin, B. Li, G. Lan, X. Q. Feng, *Proc. Natl. Acad. Sci. USA* **2017**, *114*, 8157.
[19] T. B. Saw, A. Doostmohammadi, V. Nier, L. Kocgozlu, S. Thampi, Y. Toyama, P. Marcq, C. T. Lim, J. M. Yeomans, B. Ladoux, *Nature* **2017**, *544*, 212.
[20] A. Brugués, E. Anon, V. Conte, J. H. Veldhuis, M. Gupta, J. Colombelli, J. J. Muñoz, G. W. Brodland, B. Ladoux, X. Trepat, *Nat. Phys.* **2014**, *10*, 684.
[21] M. Behrndt, G. Salbreux, P. Campinho, R. Hauschild, F. Oswald, J. Roensch, S. W. Grill, C. P. Heisenberg, *Science* **2012**, *338*, 257.
[22] Y. Shao, K. Taniguchi, K. Gurdziel, R. F. Townshend, X. F. Xue, K. M. A. Yong, J. M. Sang, J. R. Spence, D. L. Gumucio, J. P. Fu, *Nat. Mater.* **2017**, *16*, 419.
[23] A. Mongera, P. Rowghanian, H. J. Gustafson, E. Shelton, D. A. Kealhofer, E. K. Carn, F. Serwane, A. A. Lucio, J. Giammona, O. Campàs, *Nature* **2018**, *561*, 401.
[24] T. E. Angelini, E. Hannezo, X. Trepat, J. J. Fredberg, D. A. Weitz, *Phys. Rev. Lett.* **2010**, *104*, 168104.
[25] S. R. K. Vedula, M. C. Leong, T. L. Lai, P. Hersen, A. J. Kabla, C. T. Lim, B. Ladoux, *Proc. Natl. Acad. Sci. USA* **2012**, *109*, 12974.
[26] C. Blanch-Mercader, V. Yashunsky, S. Garcia, G. Duclos, L. Giomi, P. Silberzan, *Phys. Rev. Lett.* **2018**, *120*, 208101.
[27] K. Doxzen, S. R. K. Vedula, M. C. Leong, H. Hirata, N. S. Gov, A. J. Kabla, B. Ladoux, C. T. Lim, *Integr. Biol.* **2013**, *5*, 1026.
[28] D. S. Li, J. Zimmermann, H. Levine, *Phys. Biol.* **2016**, *13*, 016006.
[29] G. Duclos, C. Blanch-Mercader, V. Yashunsky, G. Salbreux, J.-F. Joanny, J. Prost, P. Silberzan, *Nat. Phys.* **2018**, *14*, 728.
[30] D. Selmeczi, S. Mosler, P. H. Hagedorn, N. B. Larsen, H. Flyvbjerg, *Biophys. J.* **2005**, *89*, 912.
[31] A. Czirok, K. Schlett, E. Madarasz, T. Vicsek, *Phys. Rev. Lett.* **1998**, *81*, 3038.
[32] L. Atia, D. Bi, Y. Sharma, J. A. Mitchel, B. Gweon, S. A. Koehler, S. J. DeCamp, B. Lan, J. H. Kim, R. Hirsch, A. F. Pegoraro, K. H. Lee, J. R. Starr, D. A. Weitz, A. C. Martin, J.-A. Park, J. P. Butler, J. J. Fredberg, *Nat. Phys.* **2018**, *14*, 613.
[33] N. Sepúlveda, L. Petitjean, O. Cochet, E. Grasland-Mongrain, P. Silberzan, V. Hakim, *PLoS Comput. Biol.* **2013**, *9*, e1002944.
[34] P. Douglas, S. Bergamini, F. Renzoni, *Phys. Rev. Lett.* **2006**, *96*, 110601.
[35] B. Liu, J. Goree, *Phys. Rev. Lett.* **2008**, *100*, 055003.

[36] R. M. Pickup, R. Cywinski, C. Pappas, B. Farago, P. Fouquet, *Phys. Rev. Lett.* **2009**, *102*, 097202.
[37] X. Trepat, M. R. Wasserman, T. E. Angelini, E. Millet, D. A. Weitz, J. P. Butler, J. J. Fredberg, *Nat. Phys.* **2009**, *5*, 426.
[38] A. J. Engler, S. Sen, H. L. Sweeney, D. E. Discher, *Cell* **2006**, *126*, 677.
[39] R. Sunyer, V. Conte, J. Escribano, A. Elosegui-Artola, A. Labernadie, L. Valon, D. Navajas, J. M. García-Aznar, J. J. Muñoz, P. Roca-Cusachs, X. Trepat, *Science* **2016**, *353*, 1157.
[40] M. Guo, A. F. Pegoraro, A. Mao, E. H. Zhou, P. R. Arany, Y. Han, D. T. Burnette, M. H. Jensen, K. E. Kasza, J. R. Moore, F. C. Mackintosh, J. J. Fredberg, D. J. Mooney, J. Lippincott-Schwartz, D. A. Weitz, *Proc. Natl. Acad. Sci. USA* **2017**, *114*, E8618.
[41] C. Bonnans, J. Chou, Z. Werb, *Nat. Rev. Mol. Cell Biol.* **2014**, *15*, 786.
[42] J. D. Humphrey, E. R. Dufresne, M. A. Schwartz, *Nat. Rev. Mol. Cell Biol.* **2014**, *15*, 802.
[43] D. E. Discher, P. Janmey, Y. L. Wang, *Science* **2005**, *310*, 1139.
[44] H. G. Yevick, G. Duclos, I. Bonnet, P. Silberzan, *Proc. Natl. Acad. Sci. USA* **2015**, *112*, 5944.
[45] W. Xi, S. Sonam, T. B. Saw, B. Ladoux, C. T. Lim, *Nat. Commun.* **2017**, *8*, 1517.
[46] T. Das, K. Safferling, S. Rausch, N. Grabe, H. Boehm, J. P. Spatz, *Nat. Cell Biol.* **2015**, *17*, 276.
[47] S. Huang, C. Brangwynne, K. Parker, D. Ingber, *Cell Motil. Cytoskeleton* **2005**, *61*, 201.
[48] K. Tanner, H. Mori, R. Mroue, A. Bruni-Cardoso, M. J. Bissell, *Proc. Natl. Acad. Sci. USA* **2012**, *109*, 1973.
[49] B. Li, S. X. Sun, *Biophys. J.* **2014**, *107*, 1532.
[50] F. J. Segerer, F. Thüroff, A. P. Alberola, E. Frey, J. O. Rädler, *Phys. Rev. Lett.* **2015**, *114*, 228102.
[51] R. Silva, A. R. Plastino, J. A. S. Lima, *Phys. Lett. A* **1998**, *249*, 401.
[52] C. Tsallis, *Braz. J. Phys.* **2009**, *39*, 337.
[53] J. H. Kim, A. F. Pegoraro, A. Das, S. A. Koehler, S. A. Ujwary, B. Lan, J. A. Mitchel, L. Atia, S. J. He, K. R. Wang, D. P. Bi, M. H. Zaman, J. A. Park, J. P. Butler, K. H. Lee, J. R. Starr, J. J. Fredberg, *Biochem. Biophys. Res. Commun.* **2020**, *521*, 706.
[54] K. A. Beningo, C. M. Lo, Y. L. Wang, *Methods Cell Biol.* **2002**, *69*, 325.
[55] J. R. Tse, A. J. Engler, *Curr. Protoc. Cell Biol.* **2010**, *47*, 10.16.1.
[56] J. N. Lee, X. Jiang, D. Ryan, G. M. Whitesides, *Langmuir* **2004**, *20*, 11684.
[57] *MATLAB and Statistics Toolbox*, The MathWorks, Inc., Natick, MA **2018**.